buildings

MDPI

*Article*

# An Improved Zonal Ventilation Control Method of Waiting Hall of High-Speed Railway Station Based on Real-Time Occupancy

**Pei Zhou [1,*], Jintao Zhou [1], Yu Tang [2], Zicheng Ma [2], Ming Yao [2], Jian Zhu [1] and Huanyu Si [1]**

[1] School of Civil Engineering, Hefei University of Technology, Hefei 230009, China; 202110593@mail.hfut.edu.cn (J.Z.); zhujian@hfut.edu.cn (J.Z.); hfutshy@163.com (H.S.)
[2] The First Company of China Eighth Engineering Bureau Ltd., Jinan 250013, China; tangzjbj@163.com (Y.T.); richen3@163.com (Z.M.); yaozjbi@163.com (M.Y.)
* Correspondence: peizhou@hfut.edu.cn

**Abstract:** The random movement of occupants in a high-speed railway station results in a more complex indoor environment. In this study, the indoor thermal environment and the thermal comfort in summer were investigated via field measurements and questionnaires in the waiting hall of a high-speed railway station. The results showed that there was an uneven horizontal temperature distribution in the area, and over 30% of the passengers were dissatisfied with the air conditioning system. In order to improve the control of the indoor temperature as well as reduce the energy consumption of the air conditioning system, an improved zonal control strategy and AMPC control optimization algorithm based on real-time people are proposed, and different control strategies are modeled and simulated using MATLAB/Simulink. It is concluded that the improved zonal control method proposed in this paper can save 28.04% of the fan energy consumption compared with the traditional control strategy.

**Keywords:** high-speed railway station; indoor thermal environment; thermal comfort; Simulink; zonal ventilation control



**Citation:** Zhou, P.; Zhou, J.; Tang, Y.; Ma, Z.; Yao, M.; Zhu, J.; Si, H. An Improved Zonal Ventilation Control Method of Waiting Hall of High-Speed Railway Station Based on Real-Time Occupancy. *Buildings* **2024**, *14*, 1783. https://doi.org/10.3390/buildings14061783

Academic Editor: Theodore Stathopoulos

Received: 17 May 2024
Revised: 4 June 2024
Accepted: 7 June 2024
Published: 13 June 2024



## 1. Introduction

According to the data released by the China National Railway Administration, the total operating mileage of the national railway reached 150,000 km in 2022, with high-speed railways accounting for a total operating mileage of 40,000 km [1]. By 2030, the total mileage of the high-speed railways in China will exceed 45,000 km, covering over 80% of the cities nationwide [2]. Modern high-speed railway station buildings, as large public buildings, have a high internal space compared to office buildings, with no internal partitions and a large flow of occupants, which results in a more complex indoor environment [3,4]. In addition, unlike other public buildings, modern high-speed railway station buildings have evolved from simple waiting areas to complex urban spaces with diverse functions and services, which has brought about issues of passengers' thermal comfort and energy consumption. Previous studies in terms of thermal comfort have shown that recommendations can be made to ensure passengers' thermal comfort in waiting areas as well as to set different thermal environment parameters to avoid unnecessary energy waste in other non-occupied areas [5,6].

Research on indoor thermal comfort has been carried out for several decades. The Predicted Mean Vote (PMV) and Percentage of People Dissatisfied (PPD) methods proposed by Fanger [7] and the adaptive model proposed by De Dear and G Brager [8] are widely used to evaluate the thermal comfort of indoor environments; high-speed railway station buildings are included as well. Chirag Deb [9] studied the indoor thermal comfort of a train station in southern India in summer, and the results showed that the passengers had a high tolerance and adaptability to the environment. Furthermore, the duration of time passengers spend in the waiting hall also affects thermal comfort [10]. In fact, passengers' adaptation to the indoor thermal environment is higher than the results predicted by the PMV–PPD model, and, with increasing time spent, passengers' real thermal neutral temperature gradually reaches

the predicted thermal neutral temperature [11]. Ye Yuan [12] investigated the dynamic thermal response of passengers throughout the departure process and determined their specific thermal comfort needs in different functional zones. The range of thermo-neutral temperature variations for passengers in different functional zones was derived by means of a questionnaire survey and calculations in order to provide a reference for improving the thermal comfort of passengers and optimizing the indoor environment.

In fact, setting the design parameters of an indoor thermal environment directly affects the thermal comfort of the indoor occupants, and it plays a vital role in the energy consumption of the building's air conditioning system. Therefore, the critical aspect to ensuring indoor thermal comfort and achieving the energy-efficient operation of the air conditioning system lies in setting appropriate indoor thermal environment parameters. However, due to the complex nature of large indoor spaces, obtaining their thermal environment parameters has become a primary concern. Currently, there are two main methods for predicting the indoor airflow and temperature distribution: micro-scale models and macro-scale models. Micro-scale models use Computational Fluid Dynamics (CFDs) based on the Navier–Stokes equations to calculate detailed indoor environments and obtain values for all the relevant parameters. However, for large indoor spaces under dynamic conditions, accurate results can be obtained but at a relatively high calculation cost [13,14]. The macro-scale models are mainly divided into node models and zone models [15]. Node models assume that the indoor environment is uniformly distributed, thereby ignoring the indoor airflow and temperature distribution. Therefore, these models can quickly simulate the dynamic changes in the thermal environment but cannot predict the complex airflow and temperature changes in large indoor spaces.

The zone model is a simulation model between the node model and CFD model, proposed by Lebrun in 1970 [16]. This model can balance the accuracy and computational cost of the model while considering the potential of multi-zone coupling, and it can predict the indoor environmental conditions easily, especially in large open-space buildings. Lu [17] proposed an adaptive zone method used in an atrium building, which can achieve similar accuracy with fewer zones compared to the traditional zoning methods. Bauman F [18] proposed a zoning model for waiting rooms that provides more accurate calculations of the load both in occupant and non-occupant zones, and the ventilation effects were evaluated, thus establishing the foundation for further energy-efficient designs.

A precise mathematical model is the fundamental aspect for achieving energy-saving control in HVAC systems. The energy-saving control in HVAC systems has made great progress in the past few decades. The most common HVAC system control method is still traditional PID control. However, when complex and variable indoor environments occur in real circumstances, the traditional PID control often cannot achieve the desired control effects. Therefore, new control methods or algorithms are continuously being developed, such as fuzzy PID control strategies [19], self-disturbance control methods [20], etc. Model predictive control (MPC) is an online optimization control algorithm with good robustness, excellent control performance, and low requirements for model accuracy. Therefore, it can be applied to optimize the building automation control systems, especially in HVAC system control [21]. In recent years, many researchers have utilized model predictive control methods for intelligent control in HVAC systems. Tang [22] proposed an MPC method for optimizing the operation of cold storage integrated central air conditioning systems during rapid DR events, which effectively reduced the building energy consumption as expected by the power grid, improved the indoor environments during DR events, and significantly reduced the indoor maximum temperatures without consuming additional energy. Wang [23] designed a gray-box coupled model for office buildings and proposed a model predictive control strategy to manage building energy consumption and indoor air quality. They also evaluated the energy-saving potential of the proposed control strategies in simulations in different climates. Ren C [24] et al. proposed a zonal demand ventilation control strategy based on a fast predictive zoning model to balance the energy savings and indoor infection rate of air conditioning systems, and the results showed that the proposed ZDCV control strategy improved the energy saving efficiency by 34% and simultaneously reduced the indoor infection rate.

This paper investigates the thermal environments of high-speed railway stations, especially for the waiting areas, adopting on-site measurements and questionnaire surveys to analyze the thermal environments in waiting areas. Additionally, an improved zoning model is employed to simulate the internal thermal environment of the target indoor space. The mathematical relationship for heat transfer within the waiting space is determined based on energy conservation principles, using real-time passenger flow data as parameters in Simulink to establish a simulation model, which is different from the previous studies. To clarify, two points that distinguish this research from the previous studies include the following: 1. in the improved zonal model, the thermal coupling effect was considered in the control model, which is different from the traditional zonal model with clear physical partitions; in this study, the zonal division is defined as virtual walls, namely without real walls or partitions. However, heat and mass transfer may occur across these virtual boundaries or between the adjacent subzones. 2. We used the real occupancy as the input of the control simulation, which can handle the supply airflow rate flexibly and maintain the indoor thermal environment to meet its requirements based on the real number of passengers. The temperature response and energy consumption under different control strategies are compared and analyzed. The rest of this paper is organized as follows: Section 2 will introduce the research methodology; the thermal environment will be summarized in Section 3, such as thermal images, indoor temperature distribution, $CO_2$ distribution, thermal sensation vote analysis, and so on; in Section 4, the mathematical model and the control algorithm will be addressed; Sections 5 and 6 include the simulation results as well as conclusions and discussions.

## 2. Research Methodology

The proposed method is shown in Figure 1, which mainly contains four parts; the first part is to obtain the parameters of the indoor thermal environment and questionnaire results through on-site measurement. The second part is to analyze the thermal indoor environment, and a zonal control strategy is proposed in this part to deal with the above issues acquired from part 1; the third part is the modeling and validation process of the proposed control strategies. The advanced control algorithm as the optimized control scheme is selected to optimize the control performance. Then, in order to verify the effectiveness of the proposed control method, the traditional zonal control method and the proposed scheme are compared and evaluated; finally, the energy consumption of the air conditioning system is predicted and compared.

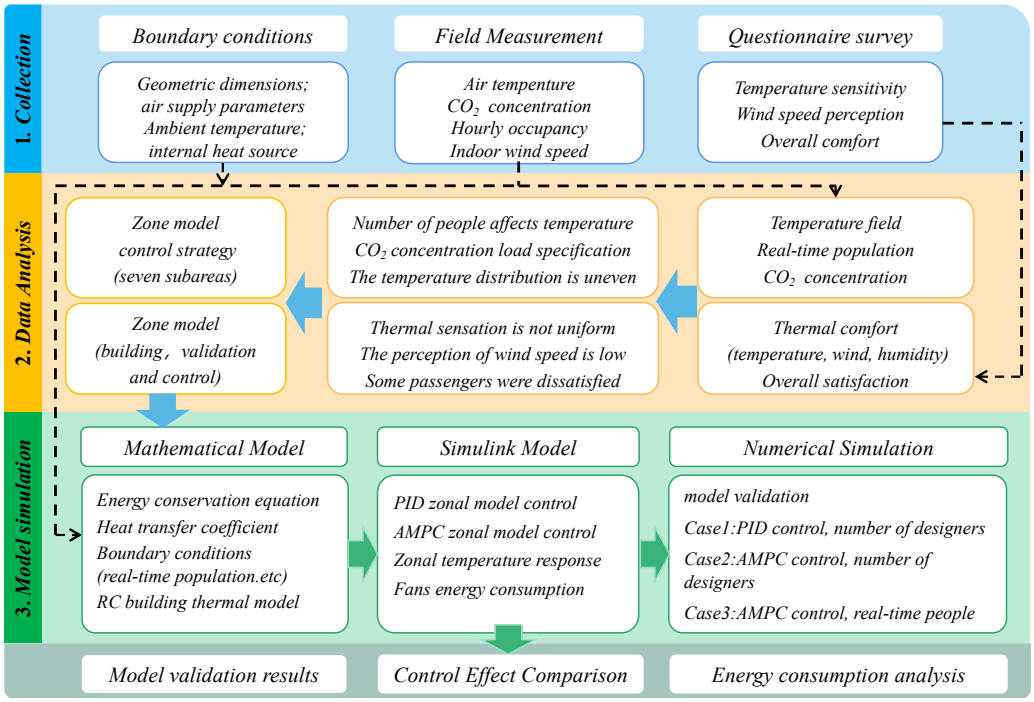


**Figure 1.** Flowchart of the research methodology.

### *2.1. Research Object and Method*

The second-floor waiting hall of the high-speed railway station is 345 m long from north to south and 145 m wide from east to west, with a total area of approximately 49,536 $m^2$. It is symmetrical from east to west, with a height of 21 m, slightly higher at the central skylight area, reaching a height of 24.4 m. The total waiting hall within the station is approximately 31,398 $m^2$. The cooling air supply inlets in the station are nozzle diffusers, with multiple of them installed parallel above the waiting area and ticket checking gates 3 m above the floor, on-site photos are shown in Figure 2 which marked as a, b, and c on the bottom.

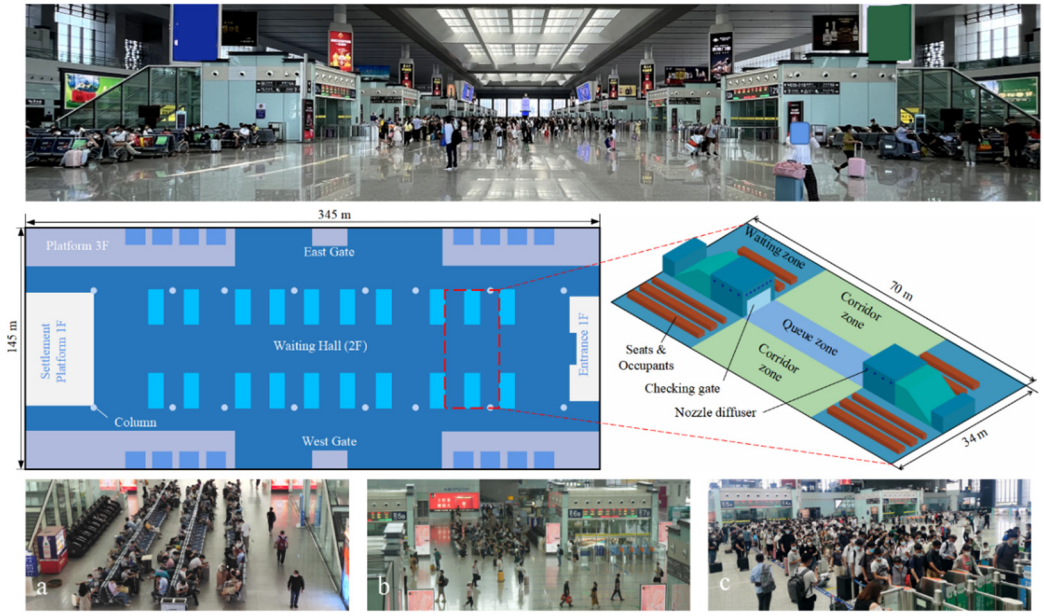


**Figure 2.** Schematic diagram and measurement area of the high-speed rail station.

Due to the large area of the waiting hall and high internal structural repetition, measurements are conducted only in the waiting areas on both sides of checking gates 4A, 5A, 4B, and 5B, as well as the central aisle. The measurement area is approximately 70 × 34 m, totaling about 2380 $m^2$. Indoor air temperature, $CO_2$ concentration, and other environmental parameters are measured. The data are collected from 7:00 to 20:30. Additionally, a questionnaire survey is conducted to gather passengers' thermal comfort perceptions and evaluations of the waiting thermal environment.

The entire measurement area is divided into three zones based on functionality: waiting zone with fixed seats, queueing zone, and aisle or corridor zone. The measured area includes two ticket checking gates and four waiting areas on both sides, with two waiting areas on each side of the gates. The aisle area is located between waiting areas on the same side, while the queueing area is between the two ticket checking gates, as illustrated in Figure 1.

#### 2.1.1. Questionnaire

This study employs the Questionnaire Star online survey platform to create electronic questionnaires, which are randomly distributed to waiting passengers within the station via QR code sharing. The questionnaire consists of over 20 questions designed to gather comprehensive information on human responses to the thermal environment. The content of the questionnaire is primarily described as follows: gender, age, thermal sensation in the current area, overall thermal comfort, etc. The thermal sensation voting in the questionnaire utilizes the ASHRAE 7-point thermal sensation scale [21], while the wind sensations are set according to the thermal sensation voting scale.

#### 2.1.2. Site Measurement of Thermal Environment

The measurement of thermal environment parameters mainly involves indoor parameter collection. The detailed parameters of the testing instruments are shown in Table 1. The measured parameters include indoor air temperature, indoor air velocity, and indoor $CO_2$ concentration. Due to the absence of obvious radiant heat sources within the measurement area, this study does not measure black globe temperature. According to ASHRAE 55 standard [25], the measurement point height is set at 1.1 m (which is breathing zone height when seated).

**Table 1.** Monitoring instruments for the thermal environment.

| Instruments | Parameters | Range | Accuracy |
|---|---|---|---|
| Thermal Imager-TiS50 | Temperature | −20~+450 °C | 0.02 °C |
| Thermal Anemometer-ST866A | Air velocity | 0~30 m/s | ±1% |
| | Air temperature | 0~45 °C | ±1 °C |
| $CO_2$ detector-AR8200 | $CO_2$ concentration | 350~9999 ppm | ±(30 + 5%) ppm |
| Laser rangefinder-DL331070L | Distance | 0.05~70 m | ±3 mm |
| Infrared thermometer-AS842A | Temperature | −50~600 °C | ±1.5 °C |

## 3. Site Measurement Analysis

### *3.1. Thermal Environment Measurement Rests*

#### 3.1.1. Overall Thermal Environment

Figure 3 shows the thermal images of different areas within the waiting hall, taken on 8 July 2022 at 10:00 a.m. with an outdoor temperature of approximately 34 °C. The captured areas include the waiting area, queueing area, and main entrance. As depicted in Figure 3, the maximum temperature difference within the captured areas exceeds 10 °C, with a maximum difference of 11.7 °C (Figure 3c) and a minimum difference of 10.2 °C (Figure 3b), indicating significant temperature variations.

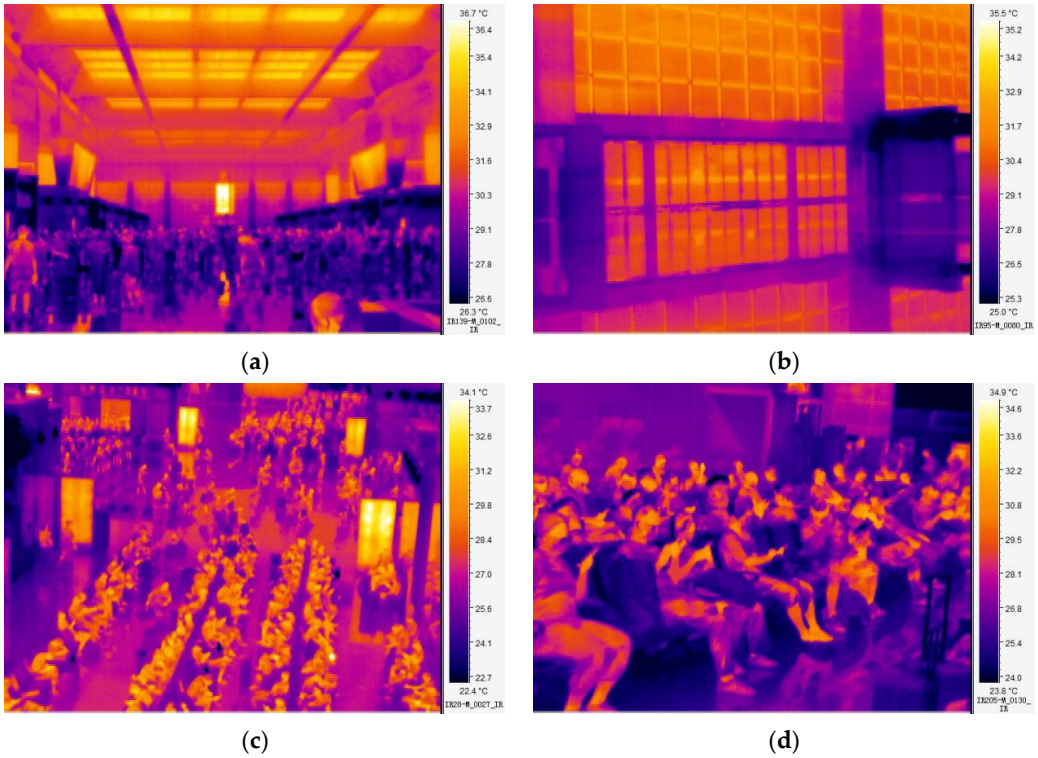

(**a**) (**b**)

(**c**) (**d**)

**Figure 3.** Thermal imaging of different areas of the waiting hall: (**a**) an overview of the waiting hall; (**b**) main entrance; (**c**) waiting area; (**d**) waiting passengers.

Figure 3a provides an overview thermal image of the waiting hall, showing a temperature difference of 10.4 °C. Temperature stratification is observed within the waiting hall, with higher temperatures in the upper space compared to the lower space, particularly noticeable from the ticket checking gate height. The station hall's ceiling is composed of glass skylights, resulting in a significant influence from outdoor conditions and overall higher temperatures in this area.

Figure 3c,d depict the temperature distribution within the waiting area. As shown in the figure, the main heat source in the waiting area is the heat generated by the flowing people, while other heat sources such as advertising boards, lighting, commercial small shops, etc., have negligible effects and can be disregarded in the following control process.

### 3.1.2. Horizontal Indoor Air Temperature Distribution

A total of 112 temperature measurement points are set up within the measurement area, with 16 points in each subzone. The overall temperature distribution within the measurement area is calculated using MATLAB's built-in linear interpolation method; the generated temperature contour is shown in Figure 4 (inwhich blue to red gradient indicating temperature increasing). The maximum measured temperature within the measurement area is 28.2 °C, while the minimum is 25.7 °C, and the maximum temperature difference is 2.3 °C. The temperature variations and zonal average temperatures are summarized in Table 2. From the figure, it can be observed that there is a significant uneven distribution of cold and hot spots within the measurement region.

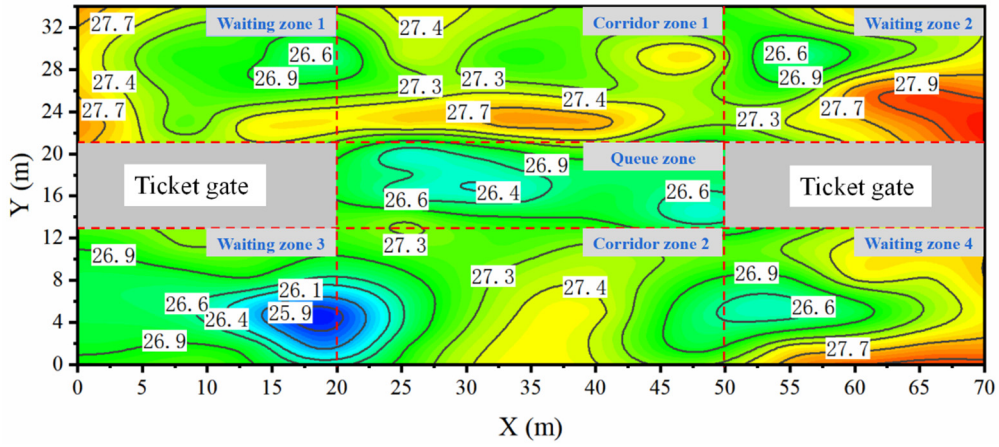


**Figure 4.** Temperature distribution in the measurement area.

**Table 2.** Measured temperature ranges and average values in each subzone.

| Measurement Area | Waiting Zone | | | | Corridor Zone | | Queue Zone |
|---|---|---|---|---|---|---|---|
| | 1 | 2 | 3 | 4 | 1 | 2 | |
| Temperature range (°C) | 26.5~27.7 | 26.5~28.2 | 26.7~27.5 | 26.5~27.8 | 27~27.8 | 26.7~27.7 | 25.7~27.3 |
| Average temperature (°C) | 27.25 | 27.5 | 26.7 | 27.4 | 27.4 | 27.15 | 26.7 |

To explore the reasons for the uneven temperature distribution within the measurement area, waiting zone 3 (waiting area 5A) is selected for temperature measurements under different conditions. The difference in the number of people is counted and measured, with three people density values set as follows: λ = 25%, λ = 50%, and λ = 75%, corresponding to approximately 20 people, 40 people, and 60 people, respectively (here, λ = 100% means designed number of passengers in this area). Five measurement points are established in waiting zone 3, and the distribution of measurement points (point 1 to 5) and temperature measurement results are shown in Figure 5.

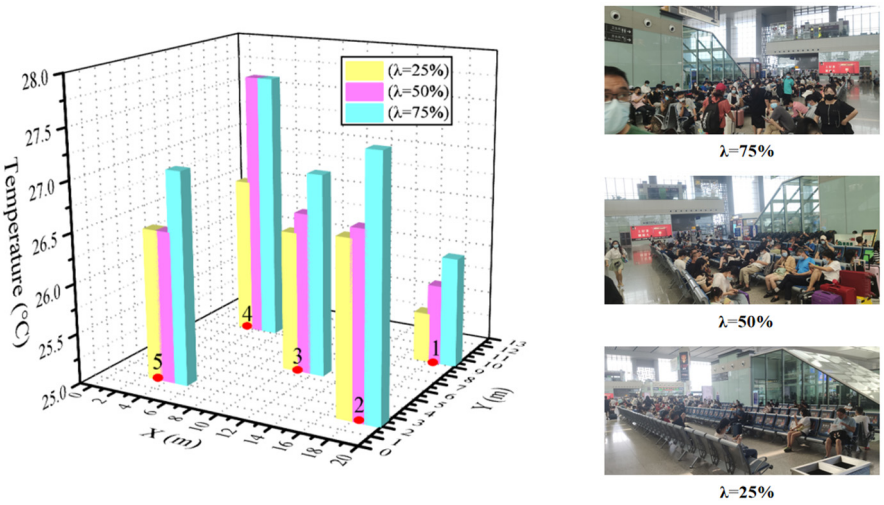


**Figure 5.** Comparison of the thermal environment of waiting zone 3 with different occupancy densities.

Figure 5 shows the temperature measurement results of waiting zone 3 under different occupancy density conditions. The X and Y axes represent the positions of the measurement points within the area, while the Z axis indicates the measured temperature. As shown in the figure, the highest measured temperature is 27.5 °C (measurement point 4, λ = 75%), and the lowest is 25.5 °C (measurement point 1, λ = 25%), with a maximum temperature difference of 2 °C. When occupancy accounts for 25% of the area, the highest measured temperature is 26.7 °C and the lowest is 25.5 °C, resulting in a temperature difference of 1.2 °C. With an occupancy rate of 50%, the temperature difference reaches 1.9 °C; the temperature difference is 1.4 °C with 75% of designed number of passengers. Under different occupancy density conditions, there is a temperature difference of over 1 °C between measurement points in waiting zone 3. Under varying occupancy densities, measurement point 1, which is closer to the air supply diffuser, consistently exhibits the lowest temperature, while measurement point 4, farther from the air supply diffuser, shows the highest temperature. Furthermore, at the same measurement point, the temperature measured when occupancy density is λ = 25% is consistently lower than when λ = 75%. Therefore, the temperature variation within the waiting zone correlates negatively with the number of occupants and their distance from the air supply diffuser. It is noted here that the air supply diffusers are operated with constant speed.

### 3.1.3. Indoor $CO_2$ Distribution

$CO_2$ concentration is one of the important factors affecting human comfort. Measurements of $CO_2$ concentration and the number of people in waiting zone 3 are conducted at different times of the day, with the measurement point located in the center of waiting zone 3 (see Figure 4), and the results are shown in Figure 6. The orange curve in the graph represents the number of people, while the blue bars represent $CO_2$ concentration. From the figure, it can be observed that, before 9:00, the number of people and $CO_2$ concentration show similar changing trends. From 10:00 to 17:00, the number of people remains relatively stable, with fluctuations of less than 10 people, and, during this period, the $CO_2$ concentration in waiting zone 3 also remains relatively stable. After 18:00, there is a significant decrease in the number of people, and, at the same time, the $CO_2$ concentration decreases slowly but follows the same decreasing trend. Therefore, there is a positive correlation between the change in $CO_2$ concentration and the change in the number of people, with a slight time lag. It is interesting that the overall $CO_2$ concentrations are less than 600 ppm, which represents a good indoor air quality (lower than the designed value, normally less than 1000 ppm); the reason for this can be explained by the tall space and opened indoor area since the $CO_2$ concentration can be easily diluted in this space.

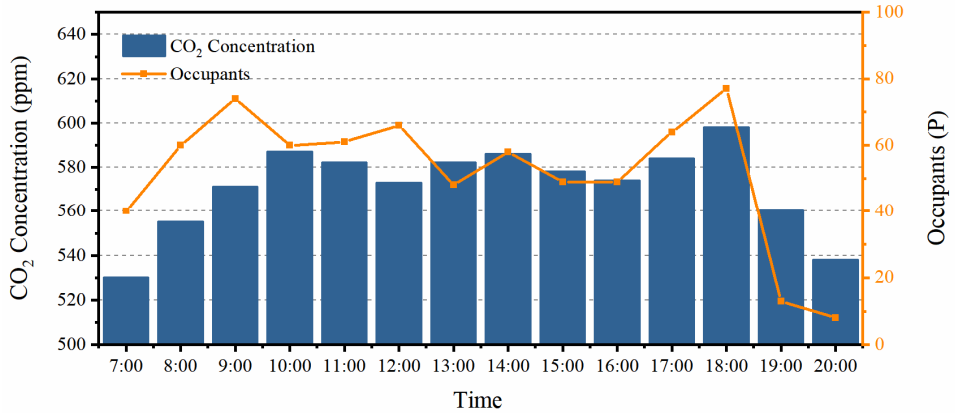


**Figure 6.** Variations in $CO_2$ concentration and number of people in waiting zone 3.

### 3.1.4. Questionnaire Results

This study collected a total of 542 valid questionnaires, including 335 males and 207 females, with a male-to-female ratio of approximately 6:4. The survey results are shown in Figure 7.

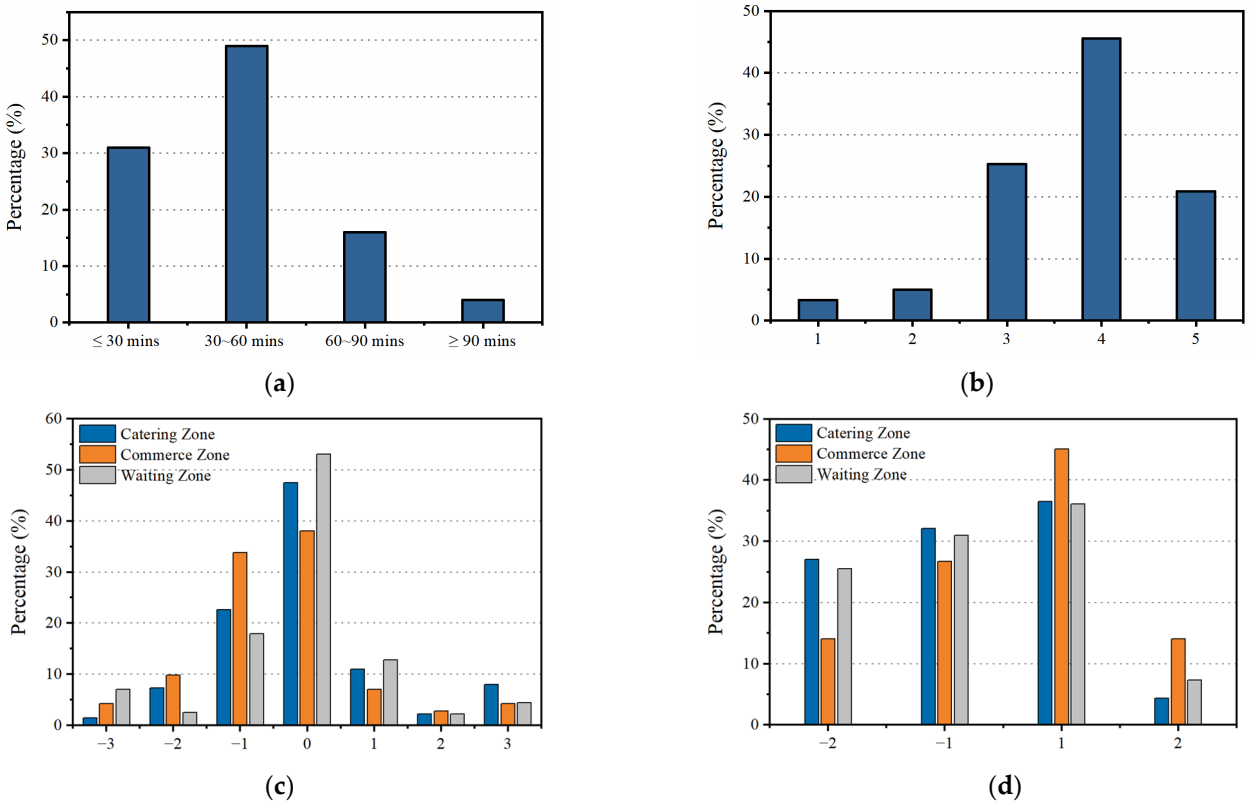


**Figure 7.** Results of the questionnaire: (**a**) waiting time for passengers; (**b**) passenger satisfaction with the air conditioning system; (**c**) thermal sensation vote; (**d**) wind sensation vote.

1. Passenger Waiting Time Statistics

Figure 7a shows the waiting times of passengers. As depicted, 35.7% of passengers have a waiting time of 30 min or less, 46.3% wait between 30 and 60 min, 13% wait between 60 and 90 min, and only 4% wait for over 90 min. Therefore, passengers generally have short waiting times at the high-speed railway stations, indicating high mobility among passengers.

2. Overall Satisfaction

Using a five-point scale, the overall satisfaction with the air conditioning system in summer is evaluated. As shown in Figure 7b, over 66% of passengers express satisfaction with the overall air conditioning system, with 45.57% rating 4 (satisfied) and 20.85% rating 5 (very satisfied). Meanwhile, among those who rated 1 to 3 points, the majority scored the air conditioning system 3 points (average), with only 3.32% expressing dissatisfaction (1 point). From the figure, it is evident that over 30% of passengers estimate the air conditioning system as average or below, indicating potential issues with temperature control in the high-speed railway station.

3. Thermal Sensation Statistics

Figure 7c displays the thermal sensation voting results of passengers in different areas of the waiting hall. As shown in the three different areas of the waiting hall, the proportion of passengers voting for neutral thermal sensation (0) is the highest. Among them, the waiting zone has the highest proportion of neutral thermal sensation, followed by the dining zone, while the commercial area's thermal sensation voting tends to lean towards slightly cool (−1) and neutral (0). Therefore, the overall thermal comfort is higher in the waiting zone, followed by the dining area, while the commercial area is generally cooler. Moreover, thermal sensation varies among passengers in different areas of the waiting hall.

4. Passenger Perception of Airflow

Figure 7d presents the voting results of passengers' perception of airflow in different areas of the waiting hall. As shown in the figure, the overall perception of airflow in each area is neutral. However, over 50% of passengers consider the airflow as too strong in both the dining and waiting areas. Moreover, the draft perception is achieved by over 40% of passengers in commercial area. Thus, the overall perception of airflow in the waiting hall is relatively high. It can be concluded that the mean thermal sensation in the dining and waiting areas is −1, indicating a perception of high airflow, while the perception of airflow in the commercial area is more balanced, with the overall thermal sensation close to neutral.

### *3.2. PMV Model*

The air temperature and indoor air velocity measured on-site are introduced into the Predicted Mean Vote (*PMV*) model proposed by ASHRAE 55-2020 [25] to calculate the *PMV* and Predicted Percentage of Dissatisfied (*PPD*) values for the four waiting areas. The calculation formulas are as follows, and the results are shown in Table 3.

$$PMV = -\frac{7}{83}T_R v_R + \frac{28}{75}T_R - \frac{689}{74} \quad (1)$$

$$PPD = 100 - 95exp(-0.03353 \cdot PMV^4 - 0.2179 \cdot PMV^2) \quad (2)$$

where $T_R$ is air temperature, °C; $v_R$ is air velocity, m/s.

**Table 3.** Calculated PMV in measuring zone.

| Measurement Area | Waiting Zone | | | | Corridor Zone | | Queue Zone |
|---|---|---|---|---|---|---|---|
| | 1 | 2 | 3 | 4 | 1 | 2 | |
| Temperature (°C) | 27.25 | 27.5 | 26.7 | 27.4 | 27.4 | 27.15 | 26.7 |
| Wind speed (m/s) | 0.40 | 0.55 | 0.79 | 0.55 | 0.28 | 0.49 | 0.90 |
| *PMV* | −0.05 | −0.32 | −1.12 | −0.35 | 0.27 | −0.29 | −1.37 |
| *PPD* | 5.05% | 7.13% | 31.43% | 7.55% | 6.51% | 6.75% | 43.92% |

ISO-7730-2005, which is an international standard of analytical determination and interpretation of thermal comfort using calculation of *PMV* and *PPD* indices and local

thermal comfort criteria [7], when the *PMV* is between −0.5 and +0.5 and the *PPD* is less than 10%, it indicates a comfortable thermal environment. From the table, it can be observed that waiting area 4 and the queueing area do not perform well in terms of thermal comfort and tend to be overall cooler. The data from the table indicate that the main reason for this is the overall high airflow velocity, while the temperature remains within the comfortable range. During on-site measurements, the air conditioning diffusers throughout the entire waiting hall are almost at full operation, especially in main stream areas within the jet flow entrainment region, leading to a strong draft sensation and more severe energy consumption.

In summary, there is a significant uneven distribution of temperature and velocity in the waiting zones of the high-speed railway station, resulting in a discrepancy in experience for passengers in terms of thermal comfort. This is evident from the survey results and *PMV* indicators, showing poor thermal comfort perception in certain waiting areas. It can be concluded that the air conditioning and ventilation strategies employed at the high-speed railway station have several issues in controlling the regional thermal environment. Therefore, in the following section, this study will use professional software to model the target space, simulate temperature response with real-time passenger flow, and further investigate the potential energy conservation of the air conditioning system with proposed control algorithms.

## 4. Mathematical Control Model

### *4.1. Model Parameters*

As shown in Figure 1, the studied area is simplified into three parts: the waiting area, the queueing area, and the aisle area. From the thermal images, it can be seen that there is a significant temperature stratification above the ticket checking gates, which are approximately 5 m high. Therefore, the height of the target area model in this study is set to 5 m. The dimensions of the waiting area (L × W × H) are 20 m × 13 m × 5 m, the queueing area is located between the two ticket checking gates, with dimensions of 30 m × 8 m × 5 m, and the aisle area has dimensions of 30 m × 13 m × 5 m.

Boundary conditions such as the wall temperature of the waiting area and the supply air temperature are measured. The air supply diffusers in the waiting area are set on both side walls, with 8 on each side. The air supply outlets in the queueing area are installed above the ticket checking gates, with a total of 14 on both sides of the gates. There are no air outlets in the aisle area. Additionally, the specifications of all air supply nozzle diffusers are consistent, with an outer geometric diameter of 0.45 m and an actual air outlet diameter of 0.25 m.

Based on the results obtained from the thermal imaging camera, the wall temperature of the waiting area is 31 °C, and the supply air temperature is 21 °C. The air supply velocity from the outlets measured by the anemometer is 4 m/s, the outdoor air temperature in the measurement area is 29 °C, and the indoor air temperature in the measurement area at 8 a.m. is 26 °C.

The determination of the number of people is particularly important as the main heat source in the study area [26]. From 8:00 a.m. to 8:00 p.m., photos are taken every 30 min to count the number of people in the waiting area, queueing area, and aisle area, resulting in 12 h of data on the changes in the number of people in the measurement area. The dynamic changes in the number of passengers in each area are shown in Figure 8. It can be observed from the figure that the number of people in the waiting area and the aisle area are relatively stable. The density of people in waiting areas 3 and 4 fluctuates around 0.33 people/$m^2$, while the density in waiting areas 1 and 2 remains stable at around 0.17 people/$m^2$. The number of people in the aisle area remains at a lower level, with an average density of only 0.04 people/$m^2$. The changes in the number of people in the queueing area are more significant. Due to the gathering of people at the ticket checking gates when the train arrives and departs, there are drastic fluctuations in the number of people, with a maximum difference exceeding 130 people. The maximum density of people

in each area at different times is 0.62 people/$m^2$, which is lower than the design density of 0.67 people/$m^2$ [27]. Therefore, traditional ventilation control strategies based on design occupancy are prone to consume more energy than those based on real-time occupancy.

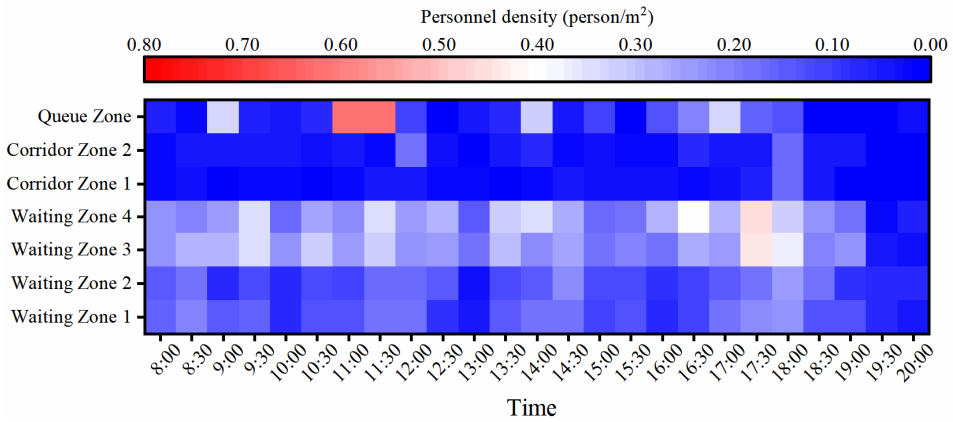


**Figure 8.** Calculation results of dynamic occupancy distribution in different areas.

### *4.2. Mathematical Model*

The measurement area of this study is located indoors with few internal devices and no obvious heat sources. Therefore, the main internal heat source is occupants. To simplify the model, other heat sources (advertising board, lighting, small shops, equipment, and heat from the ceiling level) are ignored. Thus, according to the principle of energy conservation, the simplified equation for the measurement area can be written as follows:

$$\rho C_p V \frac{dt_n}{d\tau} = \rho C_p G(t_s - t_n) + Q_1 + Q_2 \tag{3}$$

where $\rho$ is the air density in kg/$m^3$, $C_p$ is the specific heat capacity of the room in J/(kg·°C), $V$ is the volume of the room in $m^3$, $G$ is the air supply volume in $m^3$/s, $T_s$ and $T_n$ are the supply air temperature and indoor air temperature, respectively, in Celsius, $Q_1$ and $Q_2$ are, respectively, the heat transferred by the maintenance structure and the heat generated by occupant, kW. However, the spatial area of the measurement zone is separated by two ticket checking points in the middle. Moreover, since occupants are not uniformly distributed in the area but vary spatially over time, it is unreasonable to assume that the temperature distribution inside the entire area is uniform. Therefore, this model is not suitable for temperature control in the measurement area.

This paper proposes a method for coordinating temperature zoning control in large open spaces by incorporating thermal coupling effects. This method divides the large space into multiple sub-regions while considering the impact of thermal coupling effects between adjacent regions on the control of the air conditioning system [28,29]. In this study, the measurement area is divided into seven sub-regions based on their functions and load characteristics: four waiting areas, two aisle areas, and one queue area, with a total of five controllable sub-regions since there are no air vents in the aisles. Since there are no physical partitions between zones in the zoning model, when actual energy exchange occurs between adjacent zones, the heat transfer between neighboring zones may be unequal due to differences in airflow on both sides. Even with the same airflow, differences in heat transfer may occur due to turbulence, a phenomenon known as thermal coupling. In order to accurately describe the energy exchange between adjacent zones during this process, some researchers have proposed the definition of a heat exchange coefficient that can be used to represent thermal coupling between adjacent zones [30–32]:

$$Q_{\text{coup}} = k_c(t_i - t_j) \tag{4}$$

where $k_c$ is heat exchange coefficient between adjacent zones, kW/°C; $t_i$, $t_j$ is temperature of adjacent intervals, °C.

Based on Equation (4), the simplified subzone equation can be obtained accordingly; the energy conservation equation in waiting area can be written as

$$\rho C_p V \frac{dt_n}{d\tau} = \rho C_p G(t_s - t_n) + h_w A_w(t_w - t_n) + h_a A_a(t_a - t_n) + k_c(t_c - t_n) + Q \quad (5)$$

the energy conservation equation in aisle area can be written as

$$\rho C_p V \frac{dt_n}{d\tau} = h_a A_a(t_a - t_n) + k_{c,1}(t_{c,1} - t_n) + k_{c,2}(t_{c,2} - t_n) + k_{c,3}(t_{c,3} - t_n) + Q \quad (6)$$

where $\rho$ is air density, kg/m$^3$; $C_p$ is room heat capacity, kJ/(kg·°C); $V$ is room volume, m$^3$; $G$ is air supply flow-rate, (m$^3$/s); $t_w, t_a, t_c$ are side wall temperature, outside air temperature, and its adjacent zonal temperature, °C; $h_w, h_a$ represents the convective heat transfer coefficient between the side wall surface and the outside air, as well as between the air inside the waiting area and the air outside the waiting area, kW/(m$^2$·°C); $k_c$ stands for the heat exchange coefficient between the waiting area and adjacent areas, kW/°C; and $Q$ is internal heat gain generated by occupants, kW.

### *4.3. Dynamic Thermal Model*

In order to predict the thermal response of the building under given conditions (such as changes in the number of people), a dynamic thermal model of the building is developed. Detailed white-box models (the mathematical model can be directly acquired from the relationship between input and output) require high computational costs, while black-box models (the completely unknown relationship between input and output) require a large amount of data for training; therefore, this study adopts a gray-box model (the relationship between the input and output is partly known in the control system) to simulate building heat transfer. Considering that complex models increase the computational time for control simulations, the gray-box model is simplified.

The simplified model possesses both controllability and prediction accuracy; thus, it is widely used for simulating thermal changes in indoor spaces. The controlled area studied in this paper is located within the building, where solar radiation is low and there are no significant radiant heat sources; hence, radiative heat transfer can be neglected. Similar to an electrical network, the thermal changes within each sub-area can be represented by a 1R1C model. This model uses thermal resistance and thermal capacitance to represent the thermal characteristics of the building, including the building envelope, external environment, indoor air, and thermal coupling between subzones. The heat transfer between each component of the model is depicted in Figure 9. The air temperature within each sub-area is influenced by the cold air delivered by the HVAC system, external environment, internal heat gains within the sub-area, and thermal coupling between adjacent areas. Therefore, the thermal balance equations for each subzone can be revised as follows (Equations (7)–(13)):

$$C_{in,1}\frac{dT_{in,1}}{d\tau} = \frac{T_w - T_{in,1}}{R_{w,1}} + \frac{T_{out} - T_{in,1}}{R_{a,1}} + \frac{T_{in,5} - T_{in,1}}{R_{5,1}} + Q_{in,1} + Q_{HVAC,1} \quad (7)$$

$$C_{in,2}\frac{dT_{in,2}}{d\tau} = \frac{T_w - T_{in,2}}{R_{w,2}} + \frac{T_{out} - T_{in,2}}{R_{a,2}} + \frac{T_{in,5} - T_{in,2}}{R_{5,2}} + Q_{in,2} + Q_{HVAC,2} \quad (8)$$

$$C_{in,3}\frac{dT_{in,3}}{d\tau} = \frac{T_w - T_{in,3}}{R_{w,3}} + \frac{T_{out} - T_{in,3}}{R_{a,3}} + \frac{T_{in,7} - T_{in,3}}{R_{7,3}} + Q_{in,3} + Q_{HVAC,3} \quad (9)$$

$$C_{in,4}\frac{dT_{in,4}}{d\tau} = \frac{T_w - T_{in,4}}{R_{w,4}} + \frac{T_{out} - T_{in,4}}{R_{a,4}} + \frac{T_{in,7} - T_{in,4}}{R_{7,4}} + Q_{in,4} + Q_{HVAC,4} \quad (10)$$

$$C_{in,5}\frac{dT_{in,5}}{d\tau} = \frac{T_{out} - T_{in,5}}{R_{a,5}} + \frac{T_{in,1} - T_{in,5}}{R_{5,1}} + \frac{T_{in,2} - T_{in,5}}{R_{5,2}} + \frac{T_{in,6} - T_{in,5}}{R_{5,6}} + Q_{in,5} \quad (11)$$

$$C_{in,6}\frac{dT_{in,6}}{d\tau} = \frac{T_{in,5} - T_{in,6}}{R_{5,6}} + \frac{T_{in,7} - T_{in,6}}{R_{7,6}} + Q_{in,6} + Q_{HVAC,6} \quad (12)$$

$$C_{in,7}\frac{dT_{in,7}}{d\tau} = \frac{T_{out} - T_{in,7}}{R_{a,7}} + \frac{T_{in,3} - T_{in,7}}{R_{3,7}} + \frac{T_{in,4} - T_{in,7}}{R_{4,7}} + \frac{T_{in,6} - T_{in,7}}{R_{7,6}} + Q_{in,7} \quad (13)$$

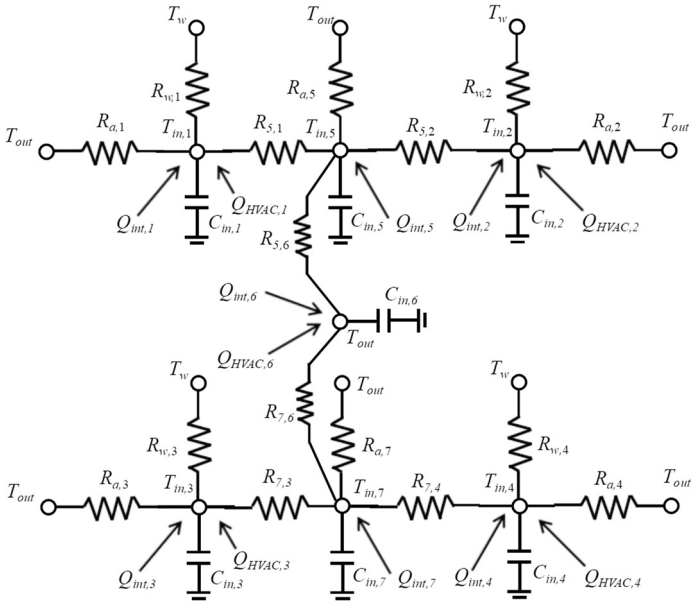


**Figure 9.** Schematic of RC gray-box building thermal model.

In the equation, $C$ and $R$, respectively, represent the thermal capacitance and thermal resistance of the model; $T$ represents temperature, with subscripts *in*, *out*, and *w* denoting the air inside each subzone, the external area, and the surface of the envelope structure, respectively; $Q_{in}$ denotes the internal heat gains of each subzone; and $Q_{HVAC}$ represents the cooling capacity provided by the HVAC system for each subzone.

The internal heat gains of the subzones are only from human body heat dissipation, and the occupants in the waiting area are in a state of light activity. According to the "Energy Efficiency Design Standard for Public Buildings [33]", the average heat dissipation per person in transportation buildings is 134 W/person. Therefore, the internal heat gain $Q_{in}$ is expressed as

$$Q_{\text{in}} = P \times q \quad (14)$$

In the equation, $P$ represents the number of occupants within the area; $q$ denotes the average heat dissipation per person, which is 134 W/per person.

Additionally, for the convenience of calculating the cooling capacity provided by the HVAC system for each subzone, it is assumed that the air inside each subzone is uniformly mixed. The cooling capacity $Q_{HVAC}$ provided by the HVAC system is calculated using the heat transfer equation:

$$Q_{HVAC,i} = \rho C G_i \left(T_{supply,i} - T_{return,i}\right) \quad (15)$$

where $\rho$, $C$ are air density and heat capacity; $G_i$ is subzone supply airflow rate, $m^3/s$; and $T_{supply,i}$, $T_{return,i}$ are zonal supply and return air temperature, °C.

It is worth noting that, at the same time, the above dynamic thermal model of the building has also been simplified: due to the controlled area being within the building, the wall temperature and surrounding environmental temperature remain relatively stable and have minimal impact on the air temperature inside; thus, they are set as constant temperatures. The heat transfer resistance between adjacent zones in the dynamic thermal model of the building is closely related to the heat exchange coefficient $k_c$ between zones, which is a function of the temperature difference between adjacent zones. Therefore, during the calculation process, the heat transfer resistance between adjacent zones varies at each time step. The adaptive model predictive control (AMPC) adopted in this study can adjust

the parameters of the model based on real-time data updates, self-correcting at each time step to improve control accuracy by correcting prediction results.

### *4.4. Air Conditioning System Control Optimization Based on Model Predictive Control*

#### 4.4.1. Control Mechanism of Adaptive Model Predictive Control

Adaptive model predictive control (AMPC) combines the principles of model predictive control (MPC) and adaptive control to handle situations where there is uncertainty, variation, or unknown parameters in the system model. The key aspect of adaptive MPC is its ability to adjust the model parameters in real time based on measurements using recursive or adaptive parameter update methods, thus continuously updating the system model to reflect changes in its dynamic behavior. Subsequently, based on the updated model and the current system state, an optimization algorithm is used to solve an optimization problem at each sampling time to compute the optimal control input sequence. The objective of the optimization problem is to minimize prediction errors while satisfying constraints to obtain the optimal control strategy. Based on the optimal control input sequence obtained, only the first control signal is applied and executed, and the process of model updating, optimization problem solving, and control signal application is repeated in the next sampling time. Through this iterative process, adaptive MPC can track real-time changes in the system's dynamic characteristics and adjust accordingly based on real-time information.

Figure 10 illustrates a schematic diagram of the AMPC for the air conditioning system in the waiting area of the high-speed railway station under real-time passenger conditions. In the structure of AMPC, the dynamic model of the system is determined based on measured boundary conditions. To obtain an adaptive model as the control model for MPC to predict the current output, the model parameters are updated and adjusted using the output results from the previous time step. Based on the prediction results, the optimal control signal for the system is determined by solving an optimization problem under the conditions of the objective function and constraints. In this study, the optimized control signal is the cooling capacity provided by the air conditioning supply fans in each area.

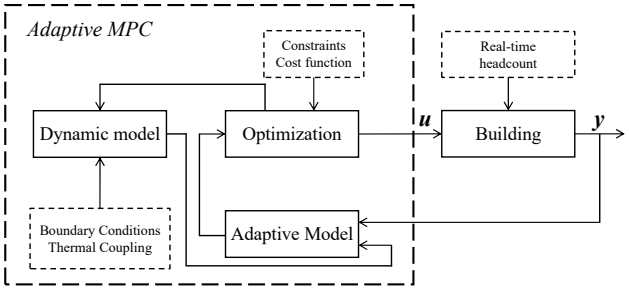


**Figure 10.** Schematic diagram of AMPC control principle based on real-time number of people.

#### 4.4.2. MPC Control Model

To establish the adaptive model predictive control controller, it is necessary to develop the dynamic thermal model of the controlled area and an adaptive model for updating model parameters. Since the issue investigated in this paper is a Multiple Input Multiple Output (MIMO) problem, a state-space model is adopted to describe the system dynamics. In order to clearly express the relationship between the inputs and outputs of the control system, the dynamic thermal model of the building (i.e., Equations (7)–(13)) is linearized and transformed into a continuous-time linear state-space model, as shown in Equation (16).

$$dx/dt = Ax + Bu \tag{16}$$

Here, system state matrix $x = [T_{in,1}, T_{in,2}, T_{in,3}, T_{in,4}, T_{in,5}, T_{in,6}, T_{in,7}]^{\mathrm{T}}$; input matrix $u = [Q_{in,i}, Q_{HVAC,i}, T_w, T_{out}]^{\mathrm{T}}$ ($i$ = 1~7). System matrix:

$$A = \begin{bmatrix} \frac{-1}{C_{in,1}\cdot R_{w,1}} + \frac{-1}{C_{in,1}\cdot R_{a,1}} + \frac{-1}{C_{in,1}\cdot R_{5,1}} & 0 & 0 & 0 \\ 0 & \frac{-1}{C_{in,2}\cdot R_{w,2}} + \frac{-1}{C_{in,2}\cdot R_{a,2}} + \frac{-1}{C_{in,2}\cdot R_{5,2}} & 0 & 0 \\ 0 & 0 & \frac{-1}{C_{in,3}\cdot R_{w,3}} + \frac{-1}{C_{in,3}\cdot R_{a,3}} + \frac{-1}{C_{in,3}\cdot R_{7,3}} & 0 \\ 0 & 0 & 0 & \frac{-1}{C_{in,4}\cdot R_{w,4}} + \frac{-1}{C_{in,4}\cdot R_{a,4}} + \frac{-1}{C_{in,4}\cdot R_{7,4}} \\ \frac{1}{C_{in,5}\cdot R_{1,5}} & \frac{1}{C_{in,5}\cdot R_{2,5}} & 0 & 0 \\ 0 & 0 & 0 & 0 \\ 0 & 0 & \frac{1}{C_{in,7}\cdot R_{7,3}} & \frac{1}{C_{in,7}\cdot R_{7,4}} \end{bmatrix}$$

$$\begin{bmatrix} \frac{1}{C_{in,1}\cdot R_{5,1}} & 0 & 0 \\ \frac{1}{C_{in,2}\cdot R_{5,2}} & 0 & 0 \\ 0 & 0 & \frac{1}{C_{in,3}\cdot R_{7,3}} \\ 0 & 0 & \frac{1}{C_{in,4}\cdot R_{7,4}} \\ \frac{-1}{C_{in,5}\cdot R_{a,5}} + \frac{-1}{C_{in,5}\cdot R_{1,5}} + \frac{-1}{C_{in,5}\cdot R_{2,5}} + \frac{-1}{C_{in,5}\cdot R_{6,5}} & \frac{1}{C_{in,5}\cdot R_{6,5}} & 0 \\ \frac{1}{C_{in,6}\cdot R_{6,5}} & \frac{-1}{C_{in,6}\cdot R_{6,5}} + \frac{-1}{C_{in,6}\cdot R_{7,6}} & \frac{1}{C_{in,6}\cdot R_{7,5}} \\ 0 & \frac{1}{C_{in,7}\cdot R_{7,6}} & \frac{-1}{C_{in,7}\cdot R_{a,7}} + \frac{-1}{C_{in,7}\cdot R_{3,7}} + \frac{-1}{C_{in,7}\cdot R_{4,7}} + \frac{-1}{C_{in,7}\cdot R_{6,7}} \end{bmatrix}_{7\times 7}$$

input matrix:

$$B = \begin{bmatrix} -\frac{1}{C_{in,1}} & 0 & 0 & 0 & 0 & 0 & 0 & \frac{1}{C_{in,1}} & 0 & 0 & 0 & 0 & 0 & 0 & \frac{1}{C_{in,1}R_{w,1}} & \frac{1}{C_{in,1}R_{a,1}} \\ 0 & -\frac{1}{C_{in,2}} & 0 & 0 & 0 & 0 & 0 & 0 & \frac{1}{C_{in,2}} & 0 & 0 & 0 & 0 & 0 & \frac{1}{C_{in,2}R_{w,2}} & \frac{1}{C_{in,2}R_{a,2}} \\ 0 & 0 & -\frac{1}{C_{in,3}} & 0 & 0 & 0 & 0 & 0 & 0 & \frac{1}{C_{in,3}} & 0 & 0 & 0 & 0 & \frac{1}{C_{in,3}R_{w,3}} & \frac{1}{C_{in,3}R_{a,3}} \\ 0 & 0 & 0 & -\frac{1}{C_{in,4}} & 0 & 0 & 0 & 0 & 0 & 0 & \frac{1}{C_{in,4}} & 0 & 0 & 0 & \frac{1}{C_{in,4}R_{w,4}} & \frac{1}{C_{in,4}R_{a,4}} \\ 0 & 0 & 0 & 0 & 0 & 0 & 0 & 0 & 0 & 0 & 0 & \frac{1}{C_{in,5}} & 0 & 0 & 0 & \frac{1}{C_{in,5}R_{a,5}} \\ 0 & 0 & 0 & 0 & 0 & -\frac{1}{C_{in,6}} & 0 & 0 & 0 & 0 & 0 & 0 & \frac{1}{C_{in,6}} & 0 & 0 & 0 \\ 0 & 0 & 0 & 0 & 0 & 0 & 0 & 0 & 0 & 0 & 0 & 0 & 0 & \frac{1}{C_{in,7}} & 0 & \frac{1}{C_{in,7}R_{a,7}} \end{bmatrix}_{7\times 16}$$

To determine the values of the block parameters, $R$ and $C$, for the dynamic thermal model, the supply air temperature, air temperature, and wall temperature in each area are recorded and fed into the model. The calculated $R$ and $C$ are shown in Table 4.

**Table 4.** Parameters of dynamic building thermal model.

| Parameter | Value (J/K) | Parameter | Value (K/W) | Parameter | Value (K/W) | Parameter | Value (K/W) |
|---|---|---|---|---|---|---|---|
| $C_{in,1}$ | $1.5756 \times 10^6$ | $R_{w,1}$ | $5.2083 \times 10^{-4}$ | $R_{a,1}$ | 0.0013 | $R_{1,5}$ | $0.5495 \times 10^{-4}$ |
| $C_{in,2}$ | $1.5756 \times 10^6$ | $R_{w,2}$ | $5.2083 \times 10^{-4}$ | $R_{a,2}$ | 0.0013 | $R_{2,5}$ | $0.5495 \times 10^{-4}$ |
| $C_{in,3}$ | $1.5756 \times 10^6$ | $R_{w,3}$ | $5.2083 \times 10^{-4}$ | $R_{a,3}$ | 0.0013 | $R_{3,7}$ | $0.5495 \times 10^{-4}$ |
| $C_{in,4}$ | $1.5756 \times 10^6$ | $R_{w,4}$ | $5.2083 \times 10^{-4}$ | $R_{a,4}$ | 0.0013 | $R_{4,7}$ | $0.5495 \times 10^{-4}$ |
| $C_{in,5}$ | $2.3634 \times 10^6$ | $R_{w,5}$ | — | $R_{a,5}$ | $5.5556 \times 10^{-4}$ | $R_{5,6}$ | $0.3571 \times 10^{-4}$ |
| $C_{in,6}$ | $1.4544 \times 10^6$ | $R_{w,6}$ | — | $R_{a,6}$ | — | $R_{6,7}$ | $0.3571 \times 10^{-4}$ |
| $C_{in,7}$ | $2.3634 \times 10^6$ | $R_{w,7}$ | — | $R_{a,7}$ | $5.5556 \times 10^{-4}$ | | |

#### 4.4.3. Model Discretization

Discretization of the model involves converting the continuous state-space building thermal model into a discrete state-space model based on sampling time, which is then applied to the MPC controller. Combining the continuous-time state-space building thermal model as shown in Equation (16) with the cooling load demand model, the discrete-time state-space model can be represented as Equations (17) and (18), which is used for predicting the evolution of the system in the MPC optimal control strategy.

$$x_{k+1} = A_d x_k + B_d u_k \tag{17}$$

$$y_k = C_d x_k \tag{18}$$

where $A_d$ and $B_d$ represent the discrete results of the system matrix $A$ and the input matrix $B$ at the sampling time, respectively; $y_k$ is the predicted result vector containing the indoor air temperatures of each subzone.

#### 4.4.4. Control Conditions

MPC control mainly consists of four parts: the objective function, constraints, system dynamics, and current state. Among these, system dynamics and current state refer to the building dynamic model and initial conditions. The objective of the MPC controller is to minimize the power consumption of the air conditioning fan under real-time passenger flow conditions. Therefore, at each time step, the objective of the MPC controller, as shown in Equation (19), is to achieve stable temperature control and minimize the air conditioning fan power demand within the prediction horizon, denoted as "$N$". The prediction horizon ($N$) at each sampling time refers to the duration from the next time step to the end of the simulated control.

$$\min J = \sum_{0}^{N-1} \left(X_{in}^{k} - X_{ref}\right)^{T} Q \left(X_{in}^{k} - X_{ref}\right) + \left(U^{K}\right)^{T} R \left(U^{K}\right) + \left(X_{in}^{N} - X_{ref}\right)^{T} F \left(X_{in}^{N} - X_{ref}\right) \tag{19}$$

where $X_{ref}$ is the setpoint for air temperature; the three terms in the equation represent the weighted sum of errors, the weighted sum of inputs, and the weighted sum of terminal errors, respectively. $Q$, $R$, and $F$ are weights assigned to each term according to the desired control effect.

The constraints of the MPC controller are defined by Equations (20) and (21), which include limits on indoor air temperature and the cooling capacity provided by the air conditioning system. Throughout the control period, the indoor air temperature is constrained to be within 0.5 °C of the setpoint, and the cooling capacity provided by the air conditioning system should not be less than 0 W. Utilizing the aforementioned objective function, inequality constraints, and discrete-time state-space model, the MPC controller is formulated as a linear optimization problem. Due to its high computational efficiency and ease of solution, it facilitates optimal control in practical applications.

$$-0.5\ ^{\circ}\mathrm{C} \leq T_{MPC}^{K} - T_{ref}^{K} \leq 0.5\ ^{\circ}\mathrm{C} \tag{20}$$

$$0\ \mathrm{W} \leq Q_{HVAC} \tag{21}$$

### *4.5. Test Platform*

This study utilizes MATLAB/Simulink software (Version R2023a) to test the designed adaptive MPC controller to optimize the control effectiveness of the air conditioning system in the high-speed railway station waiting zone under real-time passenger conditions. In Simulink, a dynamic thermal model of the waiting area is established, and the accuracy of this model is validated using site measurement results.

The initial temperature of the area is set to 26 °C, and there are a total of 8 diffusers in each waiting area. The model considers the occupants within the area as internal heat sources, and detailed parameter settings of the model can be found in Table 5.

**Table 5.** Setup of the boundary condition.

| | Waiting Zone (4) | Queue Zone | Corridor Zone (2) | Remarks |
|---|---|---|---|---|
| Room size | 20 m × 13 m × 5 m | 30 m × 8 m × 5 m | 30 m × 13 m × 5 m | |
| Supply air inlet | | Round nozzle; Φ = 0.25 m | | |
| Number of supply air inlets | 8 | 14 | — | |
| Supply airflow rate | 1.57 $m^3/s$ | 2.74 $m^3/s$ | — | |
| Supply air temperature | | 21 °C | | |
| Internal heat gains | | Occupants; 134 W/person | | [34] |
| Enclosure (checking gate) | | 31 °C | | |
| The air temperature outside the control area | | 29 °C | | |
| Heat exchange coefficient (thermal coupling) | | 280 W/($m^2$·°C) | | [30] |
| Convective heat transfer coefficient (wall with air) | | 9.6 W/($m^2$·°C) | | [35] |
| Convective heat transfer coefficient (air with air) | | 12 W/($m^2$·°C) | | [31] |

The zonal control model of the waiting area established using Simulink is shown in Figure 11. The variable air volume system (VAV) employs adaptive MPC control. The simulation time is set to 12 h, with the set temperature for each zone being $T_{ref}$ = 28 °C. The supply air temperature, $t_s$, remains at 21 °C constant. The heat source for the model is the real-time number of occupants within a 12 h period. The dynamic simulation time step is set to 1 s.

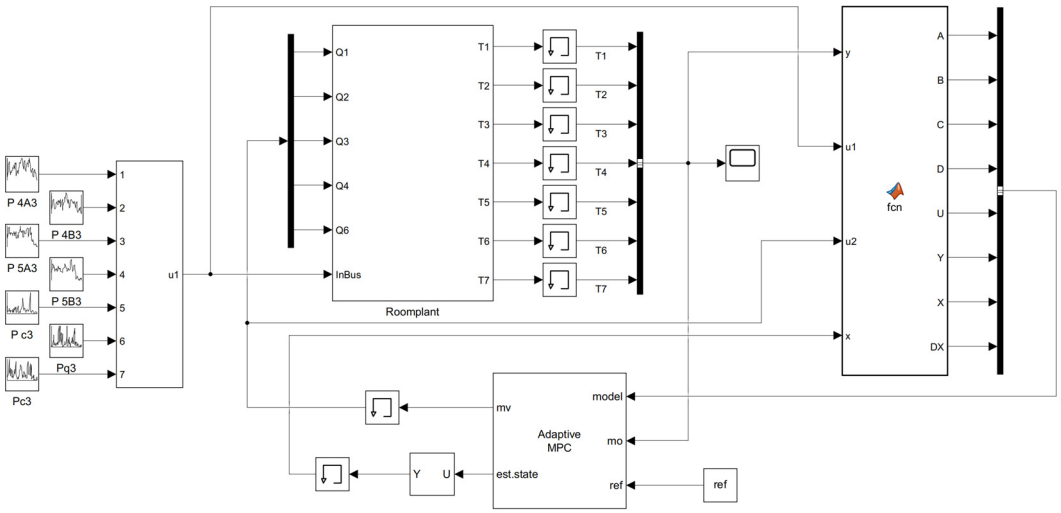


**Figure 11.** Simulation model of the measurement area.

In order to test the control performance of the proposed adaptive MPC control method and to validate the energy-saving control effect of the proposed control strategy on the operation of the air conditioning system under real-time passenger conditions, this study designed three scenarios. The specific details are shown in Table 6. Among these, the designed capacity for waiting areas 1 and 3, based on the seating arrangement within the waiting area, is 42 people, while, for waiting areas 2 and 4, it is 82 people. According to the Railway Passenger Station Design Code [36], the capacity for aisle areas is designed for 10 people, and, for queueing areas, it is designed for 40 people.

**Table 6.** Simulation scenarios.

| Cases | Controller | Internal Heat Gains |
|---|---|---|
| Case 1 | PID control | Design number of people |
| Case 2 | AMPC control | |
| Case 3 | | Real-time number of people |

## 5. Analysis of Simulation Results

### *5.1. Model Validation*

The box plots show the measured values, and the yellow lines show the predicted values. Based on the actual measurement data, the dynamic thermal model of the building is validated. A comparison between the predicted and measured temperatures of waiting area 3 is shown in Figure 12. To quantify the deviation between the predicted and measured data, two metrics are used to evaluate the predictive performance: Mean Absolute Error (MAE) and Root Mean Square Error (RMSE), as shown in Table 7. Therefore, the model established in this study can accurately simulate the temperature variations within the area and serve as a benchmark model.

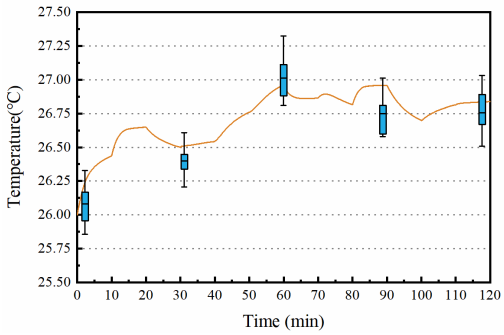


**Figure 12.** Comparison between the predicted and actual indoor air temperatures.

**Table 7.** Accuracy indices of the dynamic building thermal model.

| | MAE (°C) | RMSE (°C) |
|---|---|---|
| Indoor Air Temperature | 0.176 | 0.206 |

### *5.2. Simulation Results of Air Temperature under Different Conditions*

Based on the design conditions in Table 6, the temperature responses of each subzone are simulated and analyzed. The model parameters are consistent for each condition. The simulated temperature results of the air conditioning operation for 2 h under different conditions are shown in Figure 13.

Figure 13a shows the temperature control results of case 1. In case 1, each sub-area is independently controlled using PID controllers while considering inter-zone thermal coupling. To compare with the proposed adaptive model predictive control (AMPC) results, the temperature is set to 28 ± 0.5 °C. As shown in the figure, the temperature trends in each sub-area are basically the same, but none of them can be controlled within the design temperature range. Moreover, the temperature variations in the queueing area and the aisle area are greater than that in the waiting area, with the temperature difference in the queueing area exceeding 2 °C with variations in the number of people. Therefore, the PID controller cannot provide accurate control effects for the proposed zoning control method.

Figure 13b shows the temperature responses of each area in case 2. Case 2 adopts the adaptive model predictive control, with the control conditions as described in Section 4.4.1, and the main heat source within the area remains the design occupancy. It can be observed from the figure that, compared to the PID control, the AMPC can significantly improve the temperature control effect. After 30 min, the air temperatures in each respective area are controlled within the design temperature range. It is noted that the air temperature in the queueing area is consistently lower than in other areas, with an average temperature difference of 0.37 °C. The control setting time is approximately 11 min, with a maximum overshoot of 1.7 °C, indicating good control performance. To be more in accordance with the actual operation of the high-speed rail station's air conditioning system, the proposed AMPC control method uses the actual passenger flow in each area as the main heat source. The temperature control response of each sub-area under this

condition is shown in Figure 13c; at the beginning of the control, the temperature reaches the temperature setpoint at 12 min, with all four waiting areas reaching the designed values around 23 min. Meanwhile, under actual passenger conditions, the temperature changes when the number of people are minimal, with only the queueing area experiencing significant changes due to drastic fluctuations in the number of passengers, resulting in temperature variations exceeding the control range from 15 to 25 min and from 70 to 80 min. The aisle areas are adjacent to the queueing area, and the effect of inter-area thermal coupling causes the air temperatures in these two areas to follow the same trend as the queueing area. However, due to the lower number of people in these areas, the temperature changes exceed the set temperature limit. Therefore, under the conditions of the AMPC controller, the temperature responses of each sub-area within the waiting area are within a reasonable range, indicating an ideal temperature control effect.

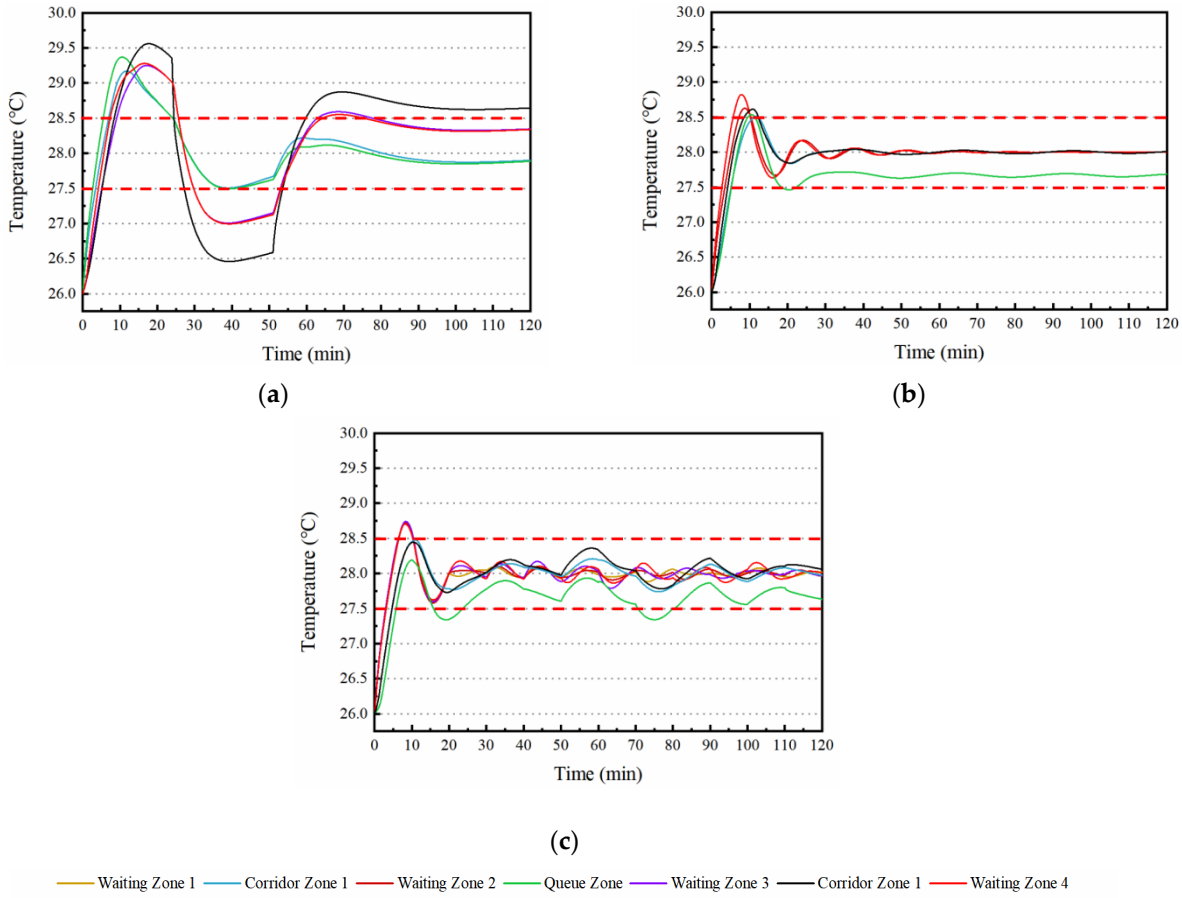


**Figure 13.** Simulation results of temperature in each area under different working conditions: (**a**) Case 1; (**b**) Case 2; (**c**) Case 3.

In conclusion, the control effect of the proposed AMPC control method is significantly better than that of the traditional PID control method. Moreover, under real-time passenger conditions, the AMPC controller can quickly control the temperature within the required range.

### *5.3. Fan Energy Consumption*

The performance of the control scenarios with actual occupancy as the heat source input undoubtedly exceeds the performance of those with design occupancy. However, the resulting issue of fan energy consumption should not be overlooked. The energy consumption of ventilation systems is directly proportional to the air volume and can be calculated using a formula in Ref. [37]. The main difference between case 1 and case 2 lies in the system's response dynamic performance indicators, while their energy con-

sumption is almost the same, so no fan energy consumption estimation is created. The total energy consumption of the fans running for 12 h in cases 2 and 3 is calculated as shown in Table 8, and the energy consumption of each area is shown in Figure 14. Using case 2 as a benchmark, the fan energy saving rate of the zoning control method based on the real-time occupancy proposed in this paper is approximately 10% to 35% (black square dot), providing an overall energy saving rate of 28.04%.

**Table 8.** Energy consumption of ventilation (12 h).

| Cases | Energy Consumption (kWh) | Energy Saving Ratio |
|---|---|---|
| Case 1 | 309.13 | — |
| Case 2 | 311.72 | — |
| Case 3 | 224.31 | 28.04% |

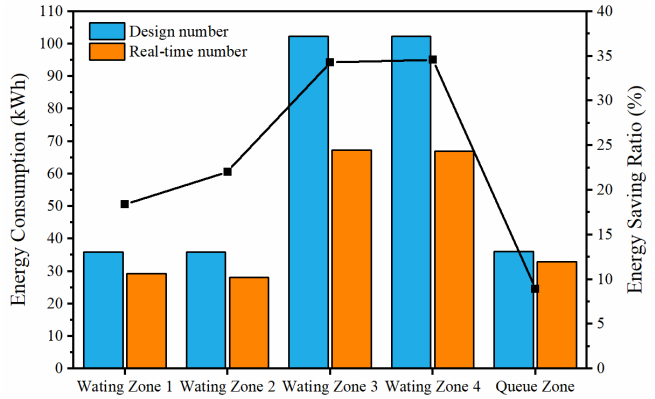


**Figure 14.** Fan energy consumption and energy saving rate (12 h).

## 6. Conclusions

This paper aims to optimize the ventilation control strategy in the high-speed rail station waiting area. The field surveys of the waiting hall revealed issues related to the thermal environment. An improved zoning model was proposed and Simulink (R2023a) software was utilized to simulate different design scenarios, and the following conclusions were drawn:

There is a significant thermal imbalance phenomenon in the high-speed rail station waiting area. The maximum temperature difference in the waiting area is 2.3 °C, mainly caused by the uneven distribution of people in the space.

This paper employs a zoning control model to simulate the dynamic temperature changes in the research area. By introducing the coefficient of heat exchange between the adjacent zones under the thermal coupling effect (which is different from the previous studies in which the zonal model has clear physical partitions), the temperature simulation results of the zoning control model are in accordance with the actual temperature measurements; thus, the proposed zoning model can accurately simulate real operating conditions.

The zoning control strategy based on real-time occupancy proposed in this paper can reduce the controller adjustment time and decrease the fan energy consumption. Compared to the traditional control methods, the comprehensive energy-saving rate is approximately 28.04%.

## 7. Limitations and Future Work

In reality, the thermal coupling process between adjacent zones is relatively complex. Factors such as turbulent flow near virtual boundaries and temperature differences can affect the value of the heat exchange coefficient. In practical processes, the heat exchange coefficient between adjacent zones should vary in real time. However, this paper's analysis is limited to validating the effectiveness of the optimization ventilation control strategy

based on the real-time occupancy in ventilation energy savings under the condition where the heat exchange coefficient varies linearly with the temperature difference between the neighboring zones. Therefore, the next stage of research needs to verify the effectiveness of the optimization control strategy under conditions where the heat exchange coefficient varies in real time due to differences in turbulence intensity and other factors. Additionally, this paper only selected one high-speed rail station as the research subject. Different high-speed rail station building layouts and dynamic changes in passengers may vary. Future applications and validations of the proposed energy-saving control strategies should be conducted in more high-speed rail buildings to improve the universality of the proposed optimization control strategies. Furthermore, the heat exchange processes between the subzones in the zoning method are complex, and there is a strong correlation among the temperature changes between the adjacent areas. The optimization algorithm used by the AMPC controller proposed in this paper cannot achieve rapid and accurate adjustment when facing complex situations. Therefore, the future research should also adopt better optimization control methods to further improve the performance of the controller, enabling the efficient energy-saving control of the ventilation and air conditioning systems in high-speed rail station waiting areas.

**Author Contributions:** Conceptualization, P.Z. and J.Z. (Jintao Zhou); methodology, P.Z.; site measurement, Y.T., Z.M., H.S., and M.Y.; control simulation, P.Z., J.Z. (Jintao Zhou), and Y.T.; writing—original draft preparation, P.Z., J.Z. (Jintao Zhou), and H.S.; writing—review and editing, Y.T., Z.M., and J.Z. (Jian Zhu), supervision, M.Y. and J.Z. (Jian Zhu), funding acquisition, Z.M. and J.Z. (Jian Zhu). All authors have read and agreed to the published version of the manuscript.

**Funding:** This work is supported by Returned Overseas Innovation and Entrepreneurship Support Program of Anhui Province (No.2022LCX020) and The National University Student Innovation and Entrepreneurship Training Program (202310359040).

**Data Availability Statement:** The data presented in this study are available in article.

**Conflicts of Interest:** Authors Yu Tang, Zicheng Ma and Ming Yao were employed by the company The First Company of China Eighth Engineering Bureau Ltd. The remaining authors declare that the research was conducted in the absence of any commercial or financial relationships that could be construed as a potential conflict of interest.

## References

1. Outline of the Fourteenth Five-Year Plan for National Economic and Social Development of the People's Republic of China and the Vision 2035. 2021. Available online: http://www.xinhuanet.com/2021-03/13/c_1127205564.htm (accessed on 7 June 2024).
2. National Development and Reform Commission. Mid-Long Term Railway Network Plan (2016–2025). Available online: https://zfxxgk.ndrc.gov.cn/web/iteminfo.jsp?id=366 (accessed on 7 June 2024). (In Chinese)
3. Lan, B.; Yu, Z.J.; Huang, G. Study on the impacts of occupant distribution on the thermal environment of tall and large public spaces. *Build. Environ.* **2022**, *218*, 109134. [CrossRef]
4. Du, X. Investigation of indoor environment comfort in large high-speed railway stations in Northern China. *Indoor Built Environ.* **2020**, *29*, 54–66. [CrossRef]
5. Su, X.; Yuan, Y.; Wang, Z.; Liu, W.; Lan, L.; Lian, Z. Human thermal comfort in non-uniform thermal environments: A review. *Energy Built Environ.* **2023**, *5*, 853–862. [CrossRef]
6. Yang, L.; Zhao, S.; Zhai, Y.; Gao, S.; Wang, F.; Lian, Z.; Duanmu, L.; Zhang, Y.; Zhou, X.; Cao, B.; et al. The Chinese thermal comfort dataset. *Sci. Data* **2023**, *10*, 662. [CrossRef]
7. *ISO 7730:2005*; Moderate Thermal Environments Determination of the PMV and PPD Indices and Specification of the Conditions for Thermal Comfort. International Organization for Standardization: Geneva, Switzerland, 2005.
8. De Dear, R.; Brager, G.S. Developing an adaptive model of thermal comfort and preference. *ASHRAE Trans.* **1998**, *104*, 145–167.
9. Deb, C.; Ramachandraiah, A. Evaluation of thermal comfort in a rail terminal location in India. *Build. Environ.* **2010**, *45*, 2571–2580. [CrossRef]
10. Wang, C.; Li, C.; Xie, L.; Wang, X.; Chang, L.; Wang, X.; Li, H.X.; Liu, Y. Thermal environment and thermal comfort in metro systems: A case study in severe cold region of China. *Build. Environ.* **2023**, *227*, 109758. [CrossRef]
11. Jia, X.; Cao, B.; Zhu, Y.; Huang, Y. Field studies on thermal comfort of passengers in airport terminals and high-speed railway stations in summer. *Build. Environ.* **2021**, *206*, 108319. [CrossRef]
12. Yuan, Y.; Yue, H.; Chen, H.; Song, C.; Liu, G. Passenger thermal comfort in the whole departure process of high-speed railway stations: A case study with thermal experience and metabolic rate changes in summer. *Energy Build.* **2023**, *291*, 113105. [CrossRef]

13. Gao, R.; Zhang, H.; Li, A.; Wen, S.; Du, W.; Deng, B. Research on optimization and design methods for air distribution system based on target values. *Build. Simul.* **2021**, *14*, 721–735. [CrossRef]
14. Wijesooriya, K.; Mohotti, D.; Lee, C.-K.; Mendis, P. A technical review of computational fluid dynamics (CFD) applications on wind design of tall buildings and structures: Past, present and future. *J. Build. Eng.* **2023**, *74*, 106828. [CrossRef]
15. Lu, Y.; Dong, J.; Liu, J. Zonal modelling for thermal and energy performance of large space buildings: A review. *Renew. Sustain. Energy Rev.* **2020**, *133*, 110241. [CrossRef]
16. Lebrun, J. Exigences Physiologiques et Modalités Physiques de la Climatisation par Source Statique Concentrée. Rédaction et Administration. 1971. Available online: https://bibliotheque.insa-lyon.fr/recherche/viewnotice/id_sigb/26801/id_int_bib/1 (accessed on 7 June 2024). (In French)
17. Lu, Y.; Wang, Z.; Liu, J.; Dong, J. Zoning strategy of zonal modeling for thermally stratified large spaces. *Build. Simul.* **2021**, *14*, 1395–1406. [CrossRef]
18. Bauman, F.S.; Dally, A. *Underfloor Air Distribution (UFAD) Design Guide*; American Society of Electroplated Plastics: Washington, DC, USA, 2003.
19. Ezber, S.; Akdoğan, E.; Gemici, Z. Fuzzy Logic Based Heating and Cooling Control in Buildings Using Intermittent Energy. In Proceedings of the International Symposium on Intelligent Manufacturing and Service Systems, Istanbul, Turkey, 26–28 May 2023; Springer: Berlin/Heidelberg, Germany, 2023.
20. Heng, L.F. Research on the Application of Self-Immunity Control Technology in the Temperature Control System of Variable Air Volume Air Conditioner. Master's Thesis, Qingdao University of Science and Technology, Qingdao, China, 2018.
21. O'Dwyer, E.; De Tommasi, L.; Kouramas, K.; Cychowski, M.; Lightbody, G. Prioritised objectives for model predictive control of building heating systems. *Control Eng. Pract.* **2017**, *63*, 57–68. [CrossRef]
22. Tang, R.; Wang, S. Model predictive control for thermal energy storage and thermal comfort optimization of building demand response in smart grids. *Appl. Energy* **2019**, *242*, 873–882. [CrossRef]
23. Wang, X.; Dong, B.; Zhang, J.J. Nationwide evaluation of energy and indoor air quality predictive control and impact on infection risk for cooling season. *Build. Simul.* **2023**, *16*, 205–223. [CrossRef] [PubMed]
24. Ren, C.; Yu, H.; Wang, J.; Zhu, H.-C.; Feng, Z.; Cao, S.-J. Zonal demand-controlled ventilation strategy to minimize infection probability and energy consumption: A coordinated control based on occupant detection. *Environ. Pollut.* **2024**, *345*, 123550. [CrossRef] [PubMed]
25. *ANSI/ASHRAE Standard 55*; Thermal Environmental Conditions for Human Occupancy. ASHRAE: Atlanta, GA, USA, 2020.
26. Wang, J.; Jiang, L.; Yu, H.; Feng, Z.; Castaño-Rosa, R.; Cao, S.-J. Computer vision to advance the sensing and control of built environment towards occupant-centric sustainable development: A critical review. *Renew. Sustain. Energy Rev.* **2024**, *192*, 114165. [CrossRef]
27. De Dear, R.J.; Brager, G.S. Thermal comfort in naturally ventilated buildings: Revisions to ASHRAE Standard 55. *Energy Build.* **2002**, *34*, 549–561. [CrossRef]
28. Huang, H.; Chen, L.; Hu, E. A neural network-based multi-zone modelling approach for predictive control system design in commercial buildings. *Energy Build.* **2015**, *97*, 86–97. [CrossRef]
29. Yang, X.; Wang, H.; Su, C.; Wang, X.; Wang, Y. Heat transfer between occupied and unoccupied zone in large space building with floor-level side wall air-supply system. *Build. Simul.* **2020**, *13*, 1221–1233. [CrossRef]
30. Zhou, P.; Wang, S.; Zhou, J.; Hussain, S.A.; Liu, X.; Gao, J.; Huang, G. A modelling method for large-scale open spaces orientated toward coordinated control of multiple air-terminal units. *Build. Simul.* **2023**, *16*, 225–241. [CrossRef] [PubMed]
31. Wang, H.; Zhou, P.; Guo, C.; Tang, X.; Xue, Y.; Huang, C. On the calculation of heat migration in thermally stratified environment of large space building with sidewall nozzle air-supply. *Build. Environ.* **2019**, *147*, 221–230. [CrossRef]
32. Zhang, S.; Cheng, Y.; Huan, C.; Lin, Z. Heat removal efficiency based multi-node model for both stratum ventilation and displacement ventilation. *Build. Environ.* **2018**, *143*, 24–35. [CrossRef]
33. *ASHRAE Handbook—Fundamentals*; ASHRAE: Atlanta, GA, USA, 2021; Available online: https://www.ashrae.org/technical-resources/ashrae-handbook/description-2021-ashrae-handbook-fundamentals (accessed on 7 June 2024).
34. *GB50189-2015*; Design Standard for Energy Efficiency of Public Buildings. Ministry of Housing and Urban-Rural Development of the People's Republic of China: Beijing, China, 2015.
35. Emmel, M.G.; Abadie, M.O.; Mendes, N. New external convective heat transfer coefficient correlations for isolated low-rise buildings. *Energy Build.* **2007**, *39*, 335–342. [CrossRef]
36. Design Code for Railway Passenger Stations. China Industry Standard-Railway CN-TB. 27 June 2018. Available online: https://www.nra.gov.cn/xwzx/xwxx/xwlb/202204/t20220405_280153.shtml (accessed on 7 June 2024).
37. Wang, J.; Huang, J.; Feng, Z.; Cao, S.-J.; Haghighat, F. Occupant-density-detection based energy efficient ventilation system: Prevention of infection transmission. *Energy Build.* **2021**, *240*, 110883. [CrossRef]